Microwave Spectrum, Structure, and Internal Motions of the Ketene–Ethylene Complex

F. J. Lovas,[†] R. D. Suenram,[†] C. W. Gillies,*[,‡] J. Z. Gillies,[§] P. W. Fowler,[⊥] and Z. Kisiel[∥]

Contribution from the Molecular Physics Division, National Institute of Standards and Technology, Gaithersburg, Maryland 20899, Departments of Chemistry, Rensselaer Polytechnic Institute, Troy, New York 12180, Siena College, Loudonville, New York 12221, and University of Exeter, Exeter EX4 4QD, U.K., and Institute of Physics, Polish Academy of Sciences, Al. Lotnikow 32/46.02 008 Warsaw, Poland

Received January 5, 1994. Revised Manuscript Received April 12, 1994[⊗]

Abstract: Microwave spectra of CH_2CO–C_2H_4, CD_2CO–C_2H_4, CH_2CO–$CH_2{=}CD_2$, CH_2CO–*cis*-CHD=CHD, and CH_2CO–*trans*-CHD=CHD have been measured with a pulsed-beam Fourier transform microwave spectrometer. A *b*-type spectrum is observed with transitions split into as many as four states due to tunneling motions which exchange the ketene hydrogens and the two pairs of hydrogens oriented *trans* to one another in ethylene. The components of the electric dipole moment along the *a* and *b* principal axes were determined to be $\mu_a = 0.160(30) \times 10^{-30}$ C m [0.048(9) D] and $\mu_b = 4.5875(33) \times 10^{-30}$ C m [1.3753(10)D]. A structure having C_s symmetry is found with ketene lying in the symmetry plane of the complex and the molecular plane of ethylene crossing the symmetry plane at 90° with a carbonyl carbon–ethylene center of mass distance, *R*, of 3.460(2) Å. Microwave and electrostatic modeling calculations show that the angle between the *b*-axis of ethylene and *R* is 49(3)°. The distributed multipole model also accounts for the planar geometry of the ketene–acetylene complex as compared to the crossed structure of the ketene–ethylene complex in terms of differences in the quadrupole moments of the two hydrocarbons. The ketene–ethylene complex has a structure which is qualitatively similar to theoretical determinations of transition-state geometries of the $CH_2CO + C_2H_4$ cycloaddition reaction. The uncertainties shown here and throughout this paper are 1σ, the standard deviation determined by least-squares fitting.

I. Introduction

Pulsed-nozzle Fourier transform microwave spectroscopy has been used to study weak intermolecular interactions in a variety of van der Waals complexes made up of unreactive monomer units.[1-3] Recently, investigations of complexes composed of reactive binding partners have appeared in the literature.[4-15] Some of these studies involve chemical species that react in the gas phase to form solids.[5-7] While van der Waals complexes were found for NH_3–HCN–HF,[5] $(CH_3)_3P$–HCl,[6] and HCN–BF_3,[14] CH_3CN–BF_3 exhibits a structure intermediate between the limits reported for van der Waals and covalently bonded systems.[10] Other work includes the ring-opening reaction of CH_2CH_2O + HCl,[7] the addition reaction of CH_3NC + HX (X = F, Cl),[11,12] and the reaction of $PH_3 + Cl_2$.[13] Weakly bound complexes formed between the two reactants were observed for each of these reactive systems.[7,11-13] A few prototypic examples of cycloaddition reactions have been studied employing dual flow mixing nozzles.[9] Bimolecular complexes were observed in $O_3 + C_2H_4$,[4] $O_3 + C_2H_2$,[9] $CH_2CO + C_2H_2$,[15] and HCNO + C_2H_2.[16]

The complexes observed in these reactive systems have properties typical of weakly bound van der Waals adducts, and there is no definitive evidence that the complexes are true chemical intermediates located in energy minima on the reaction potential surfaces.[4-9,11-16] However, the cycloaddition reactions cited above are all examples of thermally allowed concerted reactions which follow orbital symmetry rules.[17] The geometries observed for the cycloaddition complexes may be compared to reactant approaches dictated by orbital interactions and consequently to transition-state geometries determined by theoretical calculations on the reaction potential surface. Three of the reactions—$O_3 + C_2H_4$, $O_3 + C_2H_2$, and HCNO + C_2H_2—may be classified as $(2\pi_s + 4\pi_s)$ concerted cycloadditions in which the LUMO orbital of the 1,3-dipole (O_3 or HCNO) interacts with the HOMO orbital of the 1,3-dipolarophile (C_2H_4 or C_2H_2). For $O_3 + C_2H_4$ and $O_3 + C_2H_2$, a parallel approach of the two reactant molecules provides maximal overlap of the orbitals and maintains a symmetry plane along the reaction coordinate.[4,9] Hence, the approaching reactants define an envelope conformation along this reaction

[†] National Institute of Standards and Technology.
[‡] Rensselaer Polytechnic Institute.
[§] Siena College.
[⊥] University of Exeter.
[∥] Polish Academy of Science.
[⊗] Abstract published in *Advance ACS Abstracts,* May 15, 1994.

(1) Dyke, T. R. *Top. Curr. Chem.* **1984**, *120*, 86.
(2) Legon, A. C.; Millen, D. J. *Chem. Rev.* **1986**, *86*, 635.
(3) Novick, S. E. Bibliography of Rotational Spectra of Weakly Bound Complexes. In *Structure and Dynamics of Weakly Bound Molecular Complexes*; Weber, A., Ed.; Reidel Publishing Co.: Dordrecht, Holland, 1987.
(4) Gillies, J. Z.; Gillies, C. W.; Suenram, R. D.; Lovas, F. J.; Stahl, W. *J. Am. Chem. Soc.* **1989**, *111*, 3073. Gillies, C. W.; Gillies, J. Z.; Suenram, R. D.; Lovas, F. J.; Kraka, E.; Cremer, D. *J. Am. Chem. Soc.* **1991**, *113*, 2412.
(5) Emilsson, T.; Klots, T. D.; Ruoff, R. S.; Gutowsky, H. S. *J. Chem. Phys.* **1990**, *93*, 6971.
(6) Legon, A. C.; Rego, C. A. *J. Chem. Soc., Faraday Trans.* **1990**, *86*, 1915.
(7) Legon, A. C.; Rego, C. A. *Angew. Chem., Int. Ed. Engl.* **1990**, *29*, 72. Legon, A. C.; Rego, C. A. *J. Chem. Phys.* **1992**, *97*, 3050.
(8) Legon, A. C.; Warner, H. E. *J. Chem. Soc. Chem. Commun.* **1991**, 1397.
(9) Gillies, J. Z.; Gillies, C. W.; Lovas, F. J.; Matsumura, K.; Suenram, R. D.; Kraka, E.; Cremer, D. *J. Am. Chem. Soc.* **1991**, *113*, 6408.
(10) Dvorak, M. A.; Ford, R. S.; Suenram, R. D.; Lovas, F. J.; Leopold, K. R. *J. Am. Chem. Soc.* **1992**, *114*, 108.
(11) Legon, A. C.; Lister, D. G.; Warner, H. E. *Angew. Chem., Intl. Ed. Engl.* **1992**, *31*, 202.
(12) Legon, A. C.; Lister, D. G.; Warner, H. E. *J. Am. Chem. Soc.* **1992**, *114*, 8177.
(13) Legon, A. C.; Warner, H. E. *J. Chem. Phys.* **1993**, *98*, 3827.
(14) Reeve, S. W.; Burns, W. A.; Lovas, F. J.; Suenram, R. D.; Leopold, K. R. *J. Am. Chem. Soc.*, in press.
(15) Gillies, C. W.; Gillies, J. Z.; Lovas, F. J.; Suenram, R. D. *J. Am. Chem. Soc.* **1993**, *115*, 9253.
(16) Gillies, C. W.; Gillies, J. Z.; Lovas, F. J.; Suenram, R. D.; Hebert, K. 47th Symposium on Molecular Spectroscopy, Columbus, OH, 1992, Abstract RB08.
(17) Woodward, R. B.; Hoffman, R. *The Conservation of Orbital Symmetry*; Verlag Chemie GmSH: Weinheim, Germany, 1971.

0002-7863/94/1516-5285$04.50/0

coordinate. The observed geometries of the two van der Waals adducts, O_3–C_2H_4 and O_3–C_2H_2, correspond to envelope conformations in accord with the orbital symmetry analysis. Furthermore, the evidence is fairly compelling that the O_3–C_2H_4 complex falls in a shallow minimum located at large reactant distances on the reaction potential surface.[4] Finally, *ab initio* calculations show that long-range electrostatic interactions determine the binding and conformations of O_3–C_2H_4 and O_3–C_2H_2 complexes.[4,9] Therefore, it appears that the van der Waals interactions mimic the shorter range π interactions, which are important on the reaction potential surface in the vicinity of the transition state. If this is true, then geometries of van der Waals complexes in reactive systems can be used to predict transition-state structures.

In order to further investigate van der Waals complexes in cycloaddition reactions, we have studied $CH_2CO + C_2H_2$[15] previously and $CH_2CO + C_2H_4$ in the present work. van der Waals complexes of ketene cycloadditions are important because the $(2\pi_s + 2\pi_a)$ orbital interactions first discussed by Woodward and Hoffman for $CH_2CO + C_2H_4$ give a crossed transition state, **I**.[17] The molecular planes of ketene and ethylene are also mutually

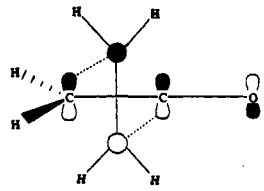

I

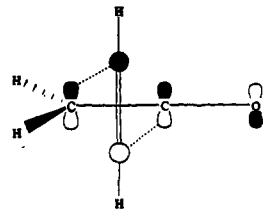

II

orthogonal to one another. Analogous $(2\pi_s + 2\pi_a)$ orbital interactions for $CH_2CO + C_2H_2$ predict a crossed transition state, **II**. Recent SCF calculations employing STO-3G basis sets describe $CH_2CO + C_2H_4$ and $CH_2CO + C_2H_2$ as concerted $(2\pi_s + 2\pi_a)$ cycloaddition reactions.[18] Complete geometry optimizations of the two transition states at the STO-3G level give structures which are crossed by approximately 25° rather than by 90° as shown above for **I** and **II**.[18] Several higher level theoretical studies also find crossed transition states for $CH_2CO + C_2H_4$.[19–22] However, there are a number of different reaction paths described that do not involve $(2\pi_s + 2\pi_a)$ orbital interactions.[19–23] In fact, two studies favor two-step processes,[20,22] and it was argued in one that orbital symmetry does not apply to the cycloaddition.[22]

In a recent microwave study of $CH_2CO + C_2H_2$, we observed the CH_2CO–C_2H_2 complex in a pulsed jet.[15] A planar structure was determined with the molecular axes of ketene and acetylene tilted by ~25° from parallel alignment and the acetylenic hydrogen oriented adjacent to the oxygen of ketene. The crossed transition-state structure calculated by SCF methods for a $(2\pi_s + 2\pi_a)$ orbital interaction[18] is clearly different from the planar complex geometry. In the present work, we report a study of the CH_2CO–C_2H_4 complex using pulsed-nozzle Fourier-transform microwave techniques. Microwave spectra of five isotopic species are used to show that the complex has a crossed structure which is qualitatively similar to the crossed transition-state geometries calculated from theory and also resembles the $(2\pi_s + 2\pi_a)$ crossed structure shown as I above. Distributed multipole analysis (DMA)[24,25] is used in the structural analysis to determine the tilt of ethylene with respect to ketene as well as to understand the observed structural differences between CH_2CO–C_2H_2 and CH_2CO–C_2H_4. Analyses of the microwave spectra also show that tunneling motions associated with the ketene and ethylene monomer units exchange the ketene hydrogens and the two pairs of *trans* ethylene hydrogens. DMA calculations find internal rotation about the *c* inertial axis of ethylene to correspond to the lowest energy pathway in agreement with the spectral results.

II. Experimental Section

The rotational spectra of the five isotopic species of the ketene–ethylene complex, CH_2CO–C_2H_4, CD_2CO–C_2H_4, CH_2CO–CH_2=CD_2, CH_2CO–*cis*-CHD=CHD, and CH_2CO–*trans*-CHD=CHD, were observed with a Fourier transform microwave spectrometer[26] employing a dual flow modified pulsed solenoid valve for the molecular beam source. Design details of the spectrometer[27] and of the modified solenoid valve[9] have been described previously. Pressurized aluminum tanks containing 1% ketene in argon and 1% ethylene in argon were used to obtain gas flows through 1.6-mm (1/16-in.) capillary tubing to the high-pressure side of the modified solenoid valve. The two gas flows mixed in the valve and exited through the normal gas input of the valve, which was connected to tubing that vented into an exhaust hood. Supersonic bursts of the gas mixture were delivered to the Fabry-Perot cavity of the spectrometer through the 0.5-mm orifice of the valve by actuating the solenoid. Digital flow controllers were used to regulate the two gas flows from the pressurized aluminum tanks through the valve.

The preparations of the two ketene isotopes were described previously.[28] Commercially available deuterium-enriched samples (99+%) of CH_2=CD_2, *cis*-CHD=CHD, and *trans*-CHD=CHD were used for the three dideuterated ethylene isotopes of the ketene–ethylene complex.

Optimum signals of transitions assigned to the ketene–ethylene complex were obtained at flow rates of 0.08 mL/s for ketene/argon and 0.17 mL/s for ethylene/argon. Stopping one or the other of these gas flows made the spectral signals disappear. Only a single gas pulse was required to observe the more intense transitions. Line centers were measured to ±4 kHz by taking the Fourier transform of the average of the FIDs (free induction decays) for 500–2000 gas pulses.

III. Results

A. Microwave Spectra. A planar geometry and conformations which cross the C=C=O axis of ketene and the C=C axis of ethylene were used to predict the rotational spectrum of CH_2–CO–C_2H_4. These structures indicate that the complex will have a prolate rotor asymmetric top spectrum with intense *b*-type R- and Q-branch transitions. The observed microwave spectrum of CH_2CO–C_2H_4 was consistent with the spectral predictions. Table 1 lists the measured frequencies and rotational quantum number assignments of the *b*-type transitions. Stark effects of many of these lines were observed and used to obtain the transition assignments. The transitions were split into as many as four components, with a large splitting of 1–2 MHz and a small splitting of up to ~130 kHz. These four components are assigned to vibrational tunneling states of CH_2CO–C_2H_4. As discussed in greater detail in Section IIID, the internal motions involve exchange of the ethylene hydrogens and exchange of the ketene hydrogens.

Table 1 gives the measured line frequencies of the four tunneling states designated A_1, A_2, B_1, and B_2. The larger A–B state splitting is due to the ethylene hydrogen exchange, while the smaller A_1–A_2 and B_1–B_2 state splittings arise from the ketene motion. Nuclear spin statistical weights expected for ketene and ethylene hydrogen exchange (see Section IIID) are listed in Table 1 under each tunneling state label. Both the 1_{11}–0_{00} and 3_{13}–2_{02} transitions exhibit only A–B splitting. The observed A/B relative intensities of these two transitions are 1.6/1.0, which agrees with the nuclear

(18) Fang, D.; Fu, X. *Beijing Shifan Daxue Xuebao. Ziran Kexueban* **1991**, *27*, 69.
(19) Wang, X.; Houk, K. N. *J. Am. Chem. Soc.* **1990**, *112*, 1754.
(20) Bernardi, F.; Bottoni, A.; Robb, M. A.; Venturini, A. *J. Am. Chem. Soc.* **1990**, *112*, 2106.
(21) Valenti, E.; Pericas, M. A.; Moyano, A. *J. Org. Chem.* **1990**, *55*, 3582.
(22) Yamabe, S.; Minato, T.; Osamura, Y. *J. Chem. Soc., Chem. Commun.* **1993**, 450.
(23) Burke, L. A. *J. Org. Chem.* **1985**, *50*, 3149.
(24) Buckingham, A. D.; Fowler, P. W. *J. Chem. Phys.* **1983**, *79*, 6426.
(25) Buckingham, A. D.; Fowler, P. W. *Can. J. Chem.* **1985**, *63*, 2018.
(26) Balle, T. J.; Flygare, W. H. *Rev. Sci. Instrum.* **1981**, *52*, 33.
(27) Lovas, F. J.; Suenram, R. D. *J. Chem. Phys.* **1987**, *87*, 2010. Suenram, R. D.; Lovas, F. J.; Fraser, G. T.; Gillies, J. Z.; Gillies, C. W.; Onda, M. *J. Mol. Spectrosc.* **1989**, *137*, 127.
(28) Cox, A. P.; Esbitt, A. S. *J. Chem. Phys.* **1963**, *38*, 1636. Jenkins, A. D. *J. Chem. Soc.* **1952**, 2563.

Table 1. Rotational Transitions of CH_2CO–C_2H_4

transition	state A_1 nuclear spin wt 5		state A_2 nuclear spin wt 15		state B_1 nuclear spin wt 3		state B_2 nuclear spin wt 9	
$J'_{K_{-1},K_{+1}}$–$J''_{K_{-1},K_{+1}}$	ν_{obsd}[a] (MHz)	$\Delta\nu$[b] (kHz)	ν_{obsd}[a] (MHz)	$\Delta\nu$[b] (kHz)	ν_{obsd}[a] (MHz)	$\Delta\nu$[b] (kHz)	ν_{obsd}[a] (MHz)	$\Delta\nu$[b] (kHz)
3_{03}–2_{12}	7755.263	1	7755.226	2	7756.326	4	7756.286	–3
5_{14}–5_{05}	8057.870	0	8057.837	0				
1_{11}–0_{00}	9460.593	–1	9460.593	–2	9459.509	–4	9459.509	–4
4_{04}–3_{13}	12 337.900	4	12 337.846	2	12 338.875	–7	12 338.875	1
2_{12}–1_{01}	13 393.268	6	13 393.259	3	13 392.187	6	13 392.187	3
3_{21}–3_{12}	15 260.750	0	15 260.791	0	15 258.295	0	15 258.342	0
2_{20}–2_{11}	15 664.798	7	15 664.744	4	15 662.265	–2	15 662.265	–1
2_{21}–2_{12}	16 581.972	–3	16 581.902	2	16 579.464	2	16 579.390	0
5_{05}–4_{14}	16 963.584	–8	16 963.522	–5	16 964.498	4	16 964.498	–3
3_{22}–3_{13}	17 054.347	11	17 054.220	3	17 051.795	–3	17 051.668	–2
3_{13}–2_{02}	17 175.398	–4	17 175.398	4	17 174.340	–6	17 174.340	–1
2_{21}–1_{10}	24 447.773	–33	24 447.706	–6	24 445.282	0	24 445.222	0
2_{20}–1_{11}			24 771.452	0			24 768.959	2

[a] The frequency measurements have an estimated uncertainty of 4 kHz. [b] $\Delta\nu$ is the observed minus calculated frequency from the least-squares fit.

Table 2. Rotation and Centrifugal Distortion Constants of CH_2CO–C_2H_4[a]

spectral constant	A_1	A_2	B_1	B_2
A (MHz)	7494.124(14)	7494.145(4)	7492.989(11)	7492.995(3)
B (MHz)	2276.628(40)	2276.643(12)	2276.613(44)	2276.410(14)
C (MHz)	1966.817(40)	1967.004(12)	1966.837(44)	1967.022(14)
Δ_J (kHz)	11.1(3)	9.70(9)	11.2(3)	9.66(10)
Δ_{JK}(kHz)	65.2(22)	72.4(7)	65.3(20)	73.4(6)
Δ_K (kHz)	–41.3(21)	–39.1(8)	–101(2)	–104.1(7)
δ_J (kHz)	1.37(7)	1.41(2)	1.98(24)	1.52(8)
δ_K (kHz)	–110(21)	–208(6)	–123(22)	–214(7)
σ (kHz)[b]	2.6	1.0	2.3	0.8

[a] The numbers given in parentheses are one standard deviation of the least-squares fit. [b] Standard deviation of the least-squares fit.

spin statistical weight A/B ratio of 20/12. Unfortunately, the expected nuclear spin statistical weight ratios of 15/5 and 9/3 for A_2/A_1 and B_2/B_1 are not as certain, because the A_1–A_2 and B_1–B_2 splittings are within the bandwidth of the microwave cavity, and consequently the intensities of the lines are critically dependent on the cavity resonance position on the mode relative to the microwave pump frequency. In spite of this problem, the A_2 and B_2 state lines are clearly at least a factor of 2 more intense than the corresponding A_1 and B_1 state lines. Therefore, the line intensities are consistent (albeit qualitatively in terms of the A_1–A_2 and B_1–B_2 pairs) with the nuclear spin statistical weights of the four states given in Table 1.

Measured transition frequencies for each tunneling state were least-squares fitted to an eight-parameter asymmetrical top Watson Hamiltonian in the I^r representation and A-reduced form.[29] The rotational constants and quartic centrifugal distortion constants obtained from these fits are listed in Table 2.

Each rotational transition of CD_2CO–C_2H_4 consisted of a doublet with a splitting of about 1 MHz. The measured line frequencies of these two states, designated A and B, are given in Table 3. Observed A/B state relative intensities of several transitions are consistent with the nuclear spin statistical weights of 10/6 due to exchange of the two equivalent pairs of hydrogens in ethylene. Consequently, the splitting is assigned to tunneling motion involving ethylene. Tunneling splittings associated with the ketene motion are not resolved due to the larger moment of inertia of CD_2CO. This is reasonable since the maximum A_1–A_2 and B_1–B_2 state splittings in CH_2CO–C_2H_4 are only about 130 kHz. Line frequencies for each state in Table 3 were fitted to the same Hamiltonian employed for the CH_2CO–C_2H_4 states, giving the molecular constants listed in Table 4.

Tunneling splittings in the rotational spectra of CH_2CO–CH_2=CD_2, CH_2CO–*cis*-CHD=CHD, and CH_2CO–*trans*-CHD=CHD are complicated by the possibility of hydrogen and deuterium exchange arising from rotation of ethylene about one of its C_2 symmetry axes. Nuclear spin statistical weights of the tunneling states for these isotopic species differ depending upon the C_2 axis in ethylene which exchanges the hydrogen and deuterium nuclei. The observed spectral splittings and nuclear spin statistical weights from relative intensities of tunneling state lines are used in Section IIID to assign the internal motion to a rotation of ethylene about its c principal axis, which is perpendicular to the molecular plane of ethylene. In addition to the ethylene internal motion, exchange of the ketene hydrogens will further split the transitions of the deuterated ethylene isotopic species of the ketene–ethylene complex.

The transitions of CH_2CO–CH_2=CD_2 were split into as many as four states. For this isotopic species, the larger splitting is reduced in comparison to CH_2CO–C_2H_4 from 1–2 MHz to about 500 kHz or less. Since the moment of inertia about the c axis of ethylene increases for the CH_2=CD_2 isotope, it is reasonable to observe a reduced splitting of the lines in the spectra of CH_2CO–CH_2=CD_2. The smaller splitting is somewhat similar to

Table 3. Rotational Transitions of CD_2CO–C_2H_4

transition	state A nuclear spin wt 10		state B nuclear spin wt 6	
$J'_{K_{-1},K_{+1}}$–$J''_{K_{-1},K_{+1}}$	ν_{obsd}[a] (MHz)	$\Delta\nu$[b] (kHz)	ν_{obsd}[a] (MHz)	$\Delta\nu$[b] (kHz)
3_{03}–2_{12}	7925.921	0	7926.467	0
1_{11}–0_{00}	8741.817	1	8741.256	1
4_{04}–3_{13}	12 373.598	1	12 374.121	0
2_{12}–1_{01}	12 504.313	–2	12 503.755	–1
4_{22}–4_{13}	13 020.568	0	13 019.268	–1
3_{21}–3_{12}	13 501.446	0	13 500.126	3
2_{20}–2_{11}	13 930.314	1	13 928.979	–2
2_{21}–2_{12}	14 936.471	–1	14 935.122	0
3_{22}–3_{13}	15 458.664	0	15 457.294	0
3_{13}–2_{02}	16 102.629	0	16 102.077	0
5_{05}–4_{14}	16 844.402	0	16 844.894	0

[a] The frequency measurements have an estimated uncertainty of 4 kHz. [b] $\Delta\nu$ is the observed minus calculated frequency in kHz from the least-squares fit.

Table 4. Rotational and Centrifugal Distortion Constants of CD_2CO–C_2H_4[a]

spectral constant	A	B
A (MHz)	6860.443(1)	6859.851(2)
B (MHz)	2222.688(3)	2222.683(5)
C (MHz)	1881.757(3)	1881.761(5)
Δ_J (kHz)	8.506(30)	8.505(4)
Δ_{JK} (kHz)	63.45(20)	63.98(26)
Δ_K (kHz)	–50.70(27)	–79.91(36)
δ_J (kHz)	1.004(31)	1.058(41)
δ_K (kHz)	–139.0(16)	–140.1(21)
σ (kHz)[b]	0.4	0.5

[a] The numbers given in parentheses are one standard deviation of the least-squares fit. [b] Overall standard deviation of the least-squares fit.

(29) Watson, J. K. G. In *Vibrational Spectra and Structure*; Durig, J. R., Ed.; Elsevier, Amsterdam, 1977; Vol. 6, p 1.

Table 5. Rotational Transitions of CH_2CO–CD_2CH_2

transition	state A_1'' nuclear spin wt 3		state A_2'' nuclear spin wt 1		state A_1' nuclear spin wt 1		state A_2' nuclear spin wt 3	
$J'_{K_{-1},K_{+1}}$–$J''_{K_{-1},K_{+1}}$	ν_{obsd}[a] (MHz)	$\Delta\nu$[b] (kHz)	ν_{obsd}[a] (MHz)	$\Delta\nu$[b] (kHz)	ν_{obsd}[a] (MHz)	$\Delta\nu$[b] (kHz)	ν_{obsd}[a] (MHz)	$\Delta\nu$[b] (kHz)
3_{03}–2_{12}	7499.223	4	7499.223	−4	7498.963	5	7498.963	6
1_{11}–0_{00}	8983.503	5	8983.503	−10	8983.783	11	8983.783	3
4_{04}–3_{13}	11 868.879	1	11 868.879	−3	11 868.621	−1	11 868.621	−2
2_{12}–1_{01}	12 780.505	3	12 780.505	−2	12 780.767	−5	12 780.767	−6
3_{21}–3_{12}	14 405.548	−1	14 405.548	−2	14 406.115	−1	14 406.115	−3
2_{20}–2_{11}	14 760.525	13	14 760.525	−6	14 761.141	12	14 761.141	11
2_{21}–2_{12}	15 558.313	−18	15 558.313	6	15 558.895	−16	15 558.895	−1
3_{22}–3_{13}	15 968.300	6	15 968.200	−3	15 968.890	6	15 968.785	3
5_{05}–4_{14}	16 282.587	0	16 282.587	1	16 282.347	0	16 282.347	0
3_{13}–2_{02}	16 446.255	−33	16 446.337	4	16 446.604	13	16 446.604	8
4_{14}–3_{03}	19 994.632	4	19 994.701	6	19 994.888	−23	19 994.949	0
2_{21}–1_{10}			23 152.722	−1			23 153.302	−14
2_{20}–1_{11}			23 433.150	7			23 433.727	4
5_{15}–4_{04}	23 447.423	2	23 447.513	−3	23 447.630	9	23 447.748	0

[a] The frequency measurements have an estimated uncertainty of 4 kHz. [b] $\Delta\nu$ is the observed minus calculated frequency from the least-squares fit.

Table 6. Rotational Transitions of CH_2CO–*cis*-CDHCDH and CH_2CO–*trans*-CDHCHD

transition	CH_2CO–*cis*-CDHCDH				CH_2CO–*trans*-CDHCHD			
	state A_1 nuclear spin wt 1		state A_2 nuclear spin wt 3		state A nuclear spin wt 15		state B nuclear spin wt 21	
$J'_{K_{-1},K_{+1}}$–$J''_{K_{-1},K_{+1}}$	ν_{obsd}[a] (MHz)	$\Delta\nu$[b] (kHz)	ν_{obsd}[a] (MHz)	$\Delta\nu$[b] (kHz)	ν_{obsd}[a] (MHz)	$\Delta\nu$[b] (kHz)	ν_{obsd}[a] (MHz)	$\Delta\nu$[b] (kHz)
3_{03}–2_{12}	7778.167	0	7778.167	4	7514.041	10	7514.282	−1
1_{11}–0_{00}	9014.198	−7	9014.198	0	8964.269	7	8963.992	−10
4_{04}–3_{13}	12 228.601	0	12 228.545	−3	11 883.115	−9	11 883.370	2
2_{12}–1_{01}	12 880.871	21	12 880.871	0	12 758.598	1	12 758.346	6
3_{21}–3_{12}	14 261.329	0	14 261.329	−3	14 350.137	2	14 349.606	1
2_{20}–2_{11}	14 623.598	2	14 623.598	7	14 706.530	1	14 705.983	−4
2_{21}–2_{12}	15 441.238	−3	15 441.156	−5	15 508.313	1	15 507.787	11
3_{22}–3_{13}	15 861.737	1	15 861.620	2	15 920.375	0	15 919.864	−2
3_{13}–2_{02}	16 613.122	−19	16 613.196	4	16 421.119	−7	16 420.881	7
5_{05}–4_{14}			16 721.215	1	16 295.783	3	16 296.013	0
4_{14}–3_{03}	20 225.630	5	20 225.694	−3	19 965.752	5	19 965.498	−3
2_{21}–1_{10}			23 174.952	−8	23 097.414	0	23 096.877	−2
2_{20}–1_{11}			23 462.848	5	23 379.355	−4	23 378.818	−4
5_{15}–4_{04}			23 741.613	1	23 414.678	−1	23 414.444	4

[a] The frequency measurements have an estimated uncertainty of 4 kHz. [b] $\Delta\nu$ is the observed minus calculated frequency from the least-squares fit.

that of CH_2CO–C_2H_4, with a maximum splitting of 110 kHz. In many lines it was not possible to identify small splittings due to the ketene tunneling motion because of the partially resolved deuterium hyperfine components. Table 5 lists the measured transition frequencies of CH_2CO–$CH_2{=}CD_2$. The designations A″ and A′ are tunneling state labels assigned to the ethylene motion, and the further splitting due to the ketene motion is identified by subscripts 1 and 2, e.g., A''_1,A''_2 or A'_1,A'_2. A number of transitions which do not exhibit A''_1,A''_2 and A'_1,A'_2 state splitting were used to determine the relative intensities of the A″/A′ states. These measurements indicate that the A″ state is slightly more intense than the A′ state. Relative intensities of the small splitting are difficult to measure, as discussed previously for CH_2CO–C_2H_4, because the two split lines fall within the bandwidth of the cavity. However, the A''_1 and A'_2 state lines are measured to be 2.8 times more intense than the A''_2 and A'_1 state lines for the 3_{22}–3_{13} transition, which is consistent with the nuclear spin statistics noted in Table 5.

Two tunneling states arising from the ketene motion were observed for CH_2CO–*cis*-CHD=CHD. As shown in Table 6, which lists the measured line frequencies, the splitting is comparable to the ketene splittings observed for CH_2CO–C_2H_4 and CH_2CO–$CH_2{=}CD_2$. While the nuclear spin weights of 1 and 3 for the two states designated A_1 and A_2, respectively, were difficult to verify due to the small spectral splitting (as discussed previously for CH_2CO–C_2H_4), the A_1 state lines were clearly less intense than the A_2 state lines. Tunneling splitting due to the ethylene motion is quenched because two structural isomers with different rotational constants are obtained for hydrogen/deuterium exchange motion about the *c* axis of ethylene for the *cis* isotope (see Section IIID).

Line frequencies of two tunneling states were measured and assigned to the ethylene internal motion for CH_2CO–*trans*-CHD=CHD. The observed splitting of the transitions was quite similar to the tunneling splitting found for CH_2CO–$CH_2{=}CD_2$ due to the ethylene internal motion. For example, the 1_{11}–0_{00} transition is split by 280 kHz in CH_2CO–$CD_2{=}CH_2$ and by 277 kHz in CH_2CO–*trans*-CHD=CHD. These two states should be further split into two components due to the ketene internal motion as observed in CH_2CO–$CH_2{=}CD_2$. Unfortunately, partially resolved deuterium hyperfine structure on transitions which exhibit additional tunneling state splitting made it difficult to obtain complete assignments of all four states. The deuterium hyperfine structure differs for the two assigned states due to the ethylene internal motion, as explained in Section IIID. Several transitions assigned to the two ethylene tunneling states exhibited no resolved hyperfine structure and no splitting from the ketene motion. Relative intensity measurements of the two tunneling state components of these lines are consistent with the nuclear spin weights of 15/21 listed in Table 6 for the A and B states, respectively.

Each tunneling state observed for the three deuterated ethylene isotopic species of the ketene–ethylene complex was fit to an I^r A-reduced Watson Hamiltonian[29] using the line frequencies listed in Tables 5 and 6. The spectral constants obtained from these fits are given in Tables 7 and 8.

B. Electric Dipole Moment. The dipole moment of CH_2CO–C_2H_4 was determined by measuring the frequency shifts as a function of the applied electric field for the Stark components of the B state 1_{11}–0_{00}, 2_{12}–1_{01}, and 3_{03}–2_{12} transitions as well as the

Table 7. Rotational and Centrifugal Distortion Constants of CH_2CO–CD_2CH_2[a]

spectral constant	A_1''	A_2''	A_1'	A_2'
A (MHz)	7084.870(28)	7084.876(7)	7085.141(21)	7085.158(9)
B (MHz)	2167.827(76)	2167.828(20)	2167.937(58)	2167.862(24)
C (MHz)	1899.185(76)	1899.121(20)	1899.083(58)	1899.156(24)
Δ_J(kHz)	8.52(53)	8.62(14)	9.30(41)	8.82(17)
Δ_{JK} (kHz)	60.5(31)	62.49(81)	56.6(24)	62.04(99)
Δ_K (kHz)	−66.1(40)	−67.8(11)	−48.5(31)	−50.6(14)
δ_J (kHz)	1.14(12)	1.203(33)	0.89(9)	1.148(41)
δ_K (kHz)	−236(40)	−234(10)	−178(31)	−215(13)
σ(kHz)[b]	6.0	1.9	4.6	2.3

[a] The numbers given in parentheses are one standard deviation of the least-squares fit. [b] Overall standard deviation of least-squares fit.

Table 8. Rotational and Centrifugal Distortion Constants of CH_2CO–*cis*-CDHCDH and CH_2CO–*trans*-CDHCHD[a]

spectral constant	CH_2CO–*cis*-CDHCDH		CH_2CO–*trans*-CDHCHD	
	A_1	A_2	A	B
A (MHz)	7080.750(26)	7080.721(6)	7066.970(7)	7066.690(9)
B (MHz)	2209.465(68)	2209.505(16)	2167.925(20)	2167.947(23)
C (MHz)	1934.066(66)	1934.035(16)	1897.823(19)	1897.801(23)
Δ_J (kHz)	8.53(58)	9.12(11)	8.92(14)	9.05(16)
Δ_{JK} (kHz)	67.2(29)	65.62(67)	61.60(8)	59.71(96)
Δ_K (kHz)	−61.0(38)	−63.29(97)	−49.5(12)	−67.5(13)
δ_J (kHz)	1.19(23)	1.201(28)	1.203(34)	1.193(71)
δ_K (kHz)	−254(36)	−229.3(84)	−213(10)	−202(12)
σ (kHz)[b]	5.2	1.6	3.7	2.2

[a] Numbers given in parentheses are one standard deviation of the least-squares fit. [b] Overall standard deviation of least-squares fit.

A state 1_{11}–0_{00} transition. As described previously,[30] static electric fields were applied to the gas bursts between two parallel plates. The effective electric field was calibrated using the J = 1–0 transition of OCS and its known dipole moment of 2.385 62(10) × 10^{-30} C m [0.71519(3) D].[31] A total of 28 measurements for seven $\Delta M_J = 0$ transitions were least-squares fit to second order perturbation theory. Fitting all three dipole components gave μ_a = 0.12(7) × 10^{-30} C m [0.036(20) D], μ_b = 4.5902(53) × 10^{-30} C m [1.3761(16) D], and $\mu_c^2 < 0$, with a residual standard deviation of 3.2 kHz. The negative value of μ_c^2 suggests that μ_c is 0. This is consistent with the symmetry of the complex which is established from the moment of inertia data in the Structural Analysis section. If μ_c is fixed at 0, refitting the data gives μ_a = 0.160(30) × 10^{-30} C m [0.048(9) D] and μ_b = 4.5875(33) × 10^{-30} C m [1.3753(10) D], with a residual standard deviation of 3.1 kHz.

C. Structural Analysis. The large inertial defect of CH_2CO–C_2H_4 in the A_1 state, $\Delta = I_c - I_a - I_b$ = −32.5 u·Å², shows that the complex has a nonplanar structure with a number of heavy atoms located out of the *a,b* plane. From the known dipole moment of ketene monomer, μ = 4.74378 × 10^{-30} C m [1.42215 D],[32] and μ_b (complex) = 4.5875 × 10^{-30} C m [1.3753 D] obtained in the present work, the projection angle of the C=C=O axis of ketene on the *b* inertial axis of the complex is calculated to be 14.7°. This shows that the C=C=O axis of ketene must be aligned nearly parallel to the *b* inertial axis of the complex. Also, the second moment, P_{cc}(complex) = $^1/_2$ $(I_a + I_b - I_c) = \sum m_i c_i^2$ = 16.23 u·Å², is close to the experimental value of I_a = 16.80 u·Å² for ethylene monomer, which means that the methylene groups of ethylene are located symmetrically out of the *a,b* plane of the complex. The hydrogens of ketene must be located in the *a,b* plane of the complex because $\Delta P_{cc} = P_{cc}(CD_2CO$–$C_2H_4) - P_{cc}(CH_2CO$–$C_2H_4)$ = 0.000 596 u·Å². Only a crossed structure as illustrated in Figure 1 is consistent with all these data.

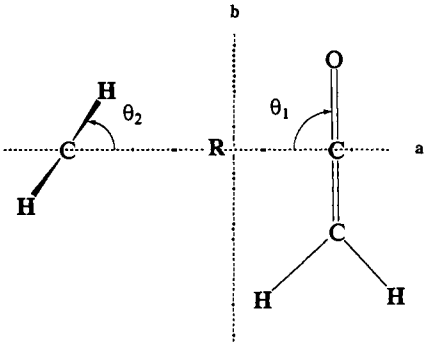

Figure 1. Structural parameters defining a crossed configuration of CH_2-CO–C_2H_4 determined from the moment of inertia data and listed in Table 12. The line, R, connecting the center of mass of ethylene and the carbonyl carbon of ketene is almost coincident with the *a* principal axis of the complex.

Table 9. Structural Parameters of CH_2CO–C_2H_4 Complex

Monomer Geometry

	distance (Å)		angle (deg)	
CH_2CO[a]	r_{CH}	1.0754	θ(HCC)	118.9
	r_{CC}	1.3147	θ(HCH)	122.2
	r_{CO}	1.1620		
C_2H_4[b]	r_{CC}	1.339	θ(HCH)	121.1
	r_{CH}	1.086		

Complex Geometry

	fit A[c] (preferred geometry)	fit B[d]
R (Å)	3.460(2)	3.461(2)
θ_1 (deg)	88(2)	89(2)
θ_2 (deg)	49(3)	130(3)
σ[e] (u·Å²)	0.57	0.58

[a] Determined from a r_o fit of the I_a and I_b moments of inertia for CH_2CO, CD_2CO, CHDCO, $^{13}CH_2CO$, and $CH_2C^{18}O$ reported in the following references. Johns, J. W. C.; Stone, J. M. R. *J. Mol. Spectrosc.* **1972**, *42*, 523. Nemes, L.; Winnewisser, M. *Z. Naturforsch* **1976**, *31a* 272. Cox, A. P.; Thomas, L. F.; Sheridan, J. *Spectrochim. Acta* **1959**, *15* 542. [b] The ethylene r_o parameters were determined from an r_o fit in the CH_2=CHD frame with use of the CH_2=CD_2, CH_2=CHD, and *cis*-CHD=CHD second moments P_{aa} and P_{bb} reported in the following reference. Hirota, E.; Endo, Y.; Saito, S.; Yoshida, K.; Yamaguchi, I.; Mochida, K. *J. Mol. Spectrosc.* **1981**, *89*, 223. [c] Fit of five isotopic species' moments of inertia with deuterium in CH_2CO–*cis*-CHD=CHD located adjacent to ketene oxygen. This geometry corresponds to the lowest energy structure obtained from DMA calculations (see Section IIIE). [d] Fit of five isotopic species' moments of inertia with deuterium in CH_2CO–*cis*-CHD=CHD located adjacent to ketene methylene group. [e] One standard deviation of the overall moment of inertia fit.

If the assumption is made that the ketene and ethylene geometries remain unchanged upon complex formation, then three coordinates are necessary to specify the crossed structure. As can be seen in Figure 1, these coordinates are R, the distance between the carbonyl carbon of ketene and the ethylene center of mass, θ_1, the angle between the ketene heavy atom axis and R, and θ_2, the angle between R and the axis defined by the C=C bond in ethylene. Moments of inertia from the ground-state rotational constants of the five isotopic species may be used in iterative least-squares fits to determine R, θ_1, and θ_2. The ground states are designated A_1 for CH_2CO–C_2H_4, A for CD_2CO–C_2H_4, A''_1 for CH_2CO–CD_2CH_2, A_1 for CH_2CO–*cis*-CHD=CHD, and A for CH_2CO–*trans*-CHD=CHD in Tables 2, 4, 6, 8. Monomer geometries are fixed at the r_o values listed in Table 9 for the moment of inertia structural analyses.

For the crossed structure shown in Figure 1, an ambiguity exists in the assignment of the observed microwave spectra of CH_2CO–*cis*-CHD=CHD. Two structurally different forms of

(30) Campbell, E. J.; Read, W. G.; Shea, J. A. *Chem. Phys. Lett.* **1983**, *94*, 69. Coudert, L. H.; Lovas, F. J.; Suenram, R. D.; Hougen, J. T. *J. Chem. Phys.* **1987**, *87*, 6290.
(31) Reinhartz, J. M. L. J.; Dymanus, A. *Chem. Phys. Lett.* **1974**, *24*, 346.
(32) Fabricant, B.; Krieger, D.; Muenter, J. S. *J. Chem. Phys.* **1977**, *67*, 1576.

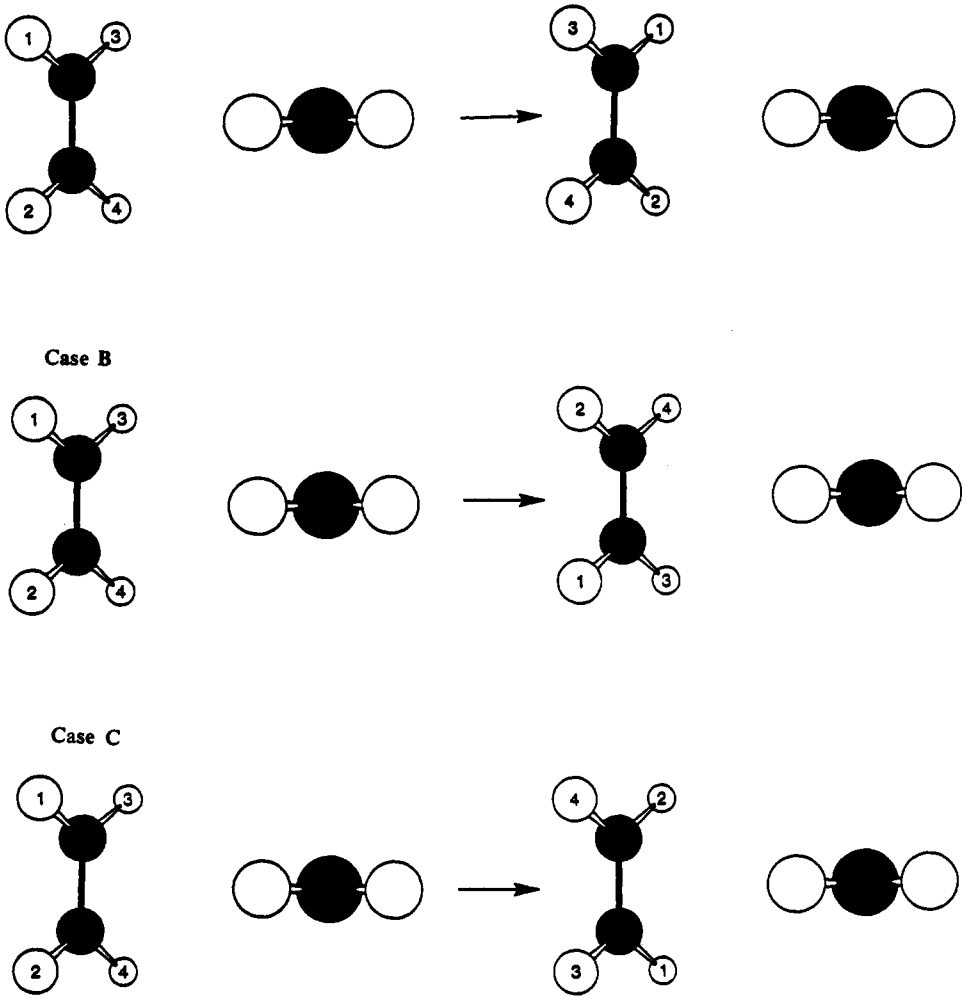

Figure 2. Three internal motions of ethylene, viewed along the *b* principal axis of the CH_2CO–C_2H_4 complex, which exchange ethylene hydrogen nuclei. The circled atoms 1, 2, 3, and 4 represent the ethylene hydrogens, while 5 and 6 are the ketene hydrogens. In cases A, B, and C, 180° rotation about the *a*, *b*, and *c* principal axes of ethylene, respectively, exchanges different pairs of ethylene hydrogens. The spectroscopic and electrostatic modeling results show that only the ethylene hydrogen exchange illustrated as case C takes place in the complex.

CH_2CO–*cis*-CHD=CHD are possible, corresponding to the deuterium atoms located either adjacent to the oxygen of ketene or adjacent to the methylene group of ketene. Since only one structural form was seen in the supersonic expansion, the observed spectrum likely arises from the lowest energy form. Analogous situations have been encountered in the related O_3–*cis*-CHD=CHD and SO_2–*cis*-CHD=CHD[33] complexes. When only one structural form is observed, it is not possible to definitively assign the observed spectra to one of the two possible forms because the rotational constants of the two forms are similar. This problem can be treated in the structural analysis by performing two least-squares fits. One, designated fit A, assigns the observed spectrum of CH_2CO–*cis*-CHD=CHD to the structural form where the deuterium atoms are located adjacent to the ketene oxygen. The second fit, designated fit B, assigns the observed spectrum to the form where the deuterium atoms are adjacent to the methylene group of ketene. Table 9 gives the two sets of values obtained for R, θ_1, and θ_2 from the two fits. Note that the geometries of structures A and B differ only in the supplementary values of θ_2. The overall standard deviations of fits A and B are 0.57 and 0.58 u·Å^2, respectively, which means that the two structures satisfy the moments of inertia of the five isotopic species equally well. Hence, it is not possible to use the moment of inertia data to distinguish between the two structures. In Section IIIE of this paper, we use a simple electrostatic model to show that structure A is more stable and corresponds to the observed ground-state spectra.

D. Internal Motions. The tunneling states observed for CH_2-CO–C_2H_4 and its four isotopic variations can be understood in terms of internal motions which exchange equivalent pairs of hydrogen and/or deuterium nuclei in ethylene and ketene. For ethylene, rotation about each of its three different C_2 axes leads to exchange of different pairs of ethylene hydrogens. Figure 2 illustrates these motions, ignoring the ketene hydrogen exchange. In case A, the two pairs of vicinal hydrogens are exchanged by 180° rotation about the *a* principal axis of ethylene (C=C bond axis). Rotation of 180° about the *b* principal axis of ethylene exchanges the two pairs of *cis* hydrogens in case B. In case C, the two pairs of *trans* hydrogens are exchanged by 180° rotation about the *c* principal axis of ethylene. In each case shown in Figure 2, tunneling through the rotational barrier gives two states. Since CH_2CO–C_2H_4 exhibits four tunneling states and the ketene hydrogen exchange produces two states, only one of the three ethylene exchange motions noted above is actually taking place in the complex. Later in this section, spectral data from the deuterated ethylene isotopic species are used to show that *trans* ethylene hydrogen exchange (case C) is the origin of the ethylene tunneling states.

Group theoretical methods described for H_2O–D_2O[30b,34] may be used to analyze the ketene and ethylene tunneling motions

(33) Andrews, A. M.; Taleb-Bendiab, A.; LaBarge, M. S.; Hillig, K. W., II; Kuczkowski, R. L. *J. Chem. Phys.* **1990**, *93*, 7030.

(34) Coudert, L. H.; Hougen, J. T. *J. Mol. Spectrosc.* **1988**, *130*, 86.

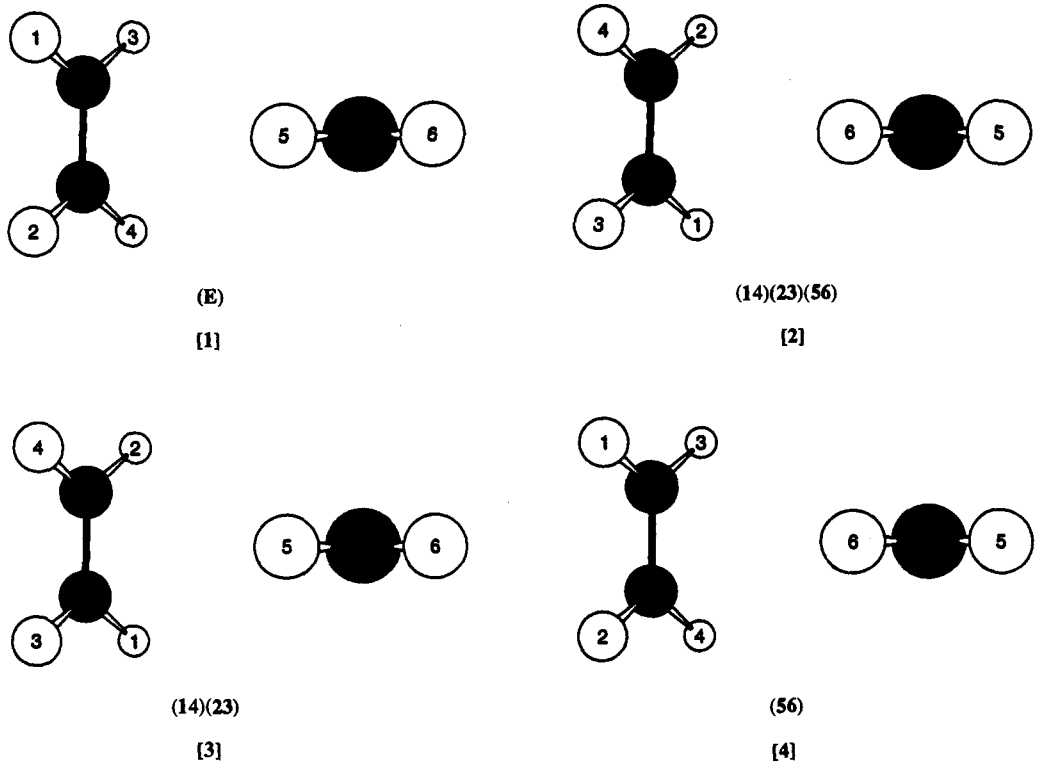

Figure 3. Four equivalent frameworks of CH_2CO–C_2H_4 designated [1], [2], [3], and [4], viewed along the *b* principal axis of the complex. The permutation inversion operation to be applied upon the basis function of framework [1] is given in parentheses under that framework. Note that only the ethylene hydrogen exchange depicted by case C in Figure 2 is represented by these four frameworks.

described above for the ketene–ethylene complex. For a crossed structure with a plane of symmetry, four equivalent configurations exist for CH_2CO–C_2H_4. These nonsuperimposable frameworks are designated [1], [2], [3], and [4] in Figure 3. Pathway [1] → [4] exchanges the ketene hydrogens by tunneling through a barrier to internal rotation about the *a* principal axis of ketene. The two pairs of trans ethylene hydrogens (case C in Figure 2) are exchanged in pathway [1] → [3] by tunneling through an internal rotation barrier about the *c* principal axis in ethylene. A concerted tunneling of both the ketene and the ethylene hydrogens is depicted as a geared motion in pathway [1] → [2].

Tunneling between the four frameworks in Figure 3 splits each asymmetric rotational energy level into four states. The four states belong to symmetry species $A^{\pm}_1$, $A^{\pm}_2$, $B^{\pm}_1$, and $B^{\pm}_2$ and obey the selection rules $A^{\pm}_1 \leftrightarrow A^{\pm}_1$, $A^{\pm}_2 \leftrightarrow A^{\pm}_2$, $B^{\pm}_1 \leftrightarrow B^{\pm}_1$, and $B^{\pm}_2 \leftrightarrow B^{\pm}_2$. In agreement with this analysis, the observed *b*-type transitions follow pure rotation selection rules and take place entirely within a particular tunneling state. Exchange of the two pairs of ethylene hydrogens gives nuclear spin weights of 10:6 for the A:B states. Ketene exchange leads to overall nuclear spin weights of 5:15:3:9 for A_1:A_2:B_1:B_2. These spin weights are consistent with the observed relative intensities of transitions from the four states.

Nuclear spin statistics for the deuterated ethylene-ketene isotopic species can be used in conjunction with measurements of relative intensities of lines from the tunneling states to show that the ethylene tunneling splitting arises from *trans* hydrogen exchange (case C, Figure 2). The effect of ethylene hydrogen and deuterium exchange without ketene exchange is considered first in the analysis of the spin statistics. This approach is useful because the ketene tunneling splitting is not resolved for many transitions and intensity measurements of these transitions can be directly compared to the ethylene exchange spin statistics. Table 10 summarizes the nuclear spin statistics of CH_2CO–CD_2-CH_2, CH_2CO–*trans*-CHD=CHD, and CH_2CO–*cis*-CHD=CHD for the three ethylene internal motions described as cases A, B, and C in Figure 2.

The nuclear spin statistics for CH_2CO–C_2H_4 are not dependent upon the ethylene tunneling exchange in case A, B, or C. However, comparison of the nuclear spin statistics for the deuterated ethylene species in Table 10 shows that spin weights of 15:21 are expected for only one isotopic species undergoing a particular ethylene tunneling motion. For example, the ethylene exchange motion in case C (ignoring the ketene motion) gives two equivalent frameworks for CH_2CO–*trans*-CHD=CHD and hence two tunneling states, A:B, with spin statistics of 15:21. Consideration of the ketene hydrogen exchange increases the number of tunneling states to four, A_1:A_2:B_1:B_2, and modifies the spin statistics to 5:15:7:21. The same analysis applied to CH_2CO–CH_2=CD_2 for case C leads to different results. Here the ethylene motion exchanges each hydrogen with a deuterium, which does not yield two equivalent frameworks. Hence, the ethylene motion produces two tunneling states designated A″:A′ of equal spin weights. These states are further split by the ketene motion to give four states, A_1″:A_2″:A_1′:A_2′, with spin weights of 1:3:1:3. Finally, CH_2CO–*cis*-CHD=CHD is unique among these isotopic species in that the ethylene motion for case C gives structurally nonequivalent species with different rotational constants. Hence the ethylene tunneling motion is quenched for CH_2CO–*cis*-CHD=CHD. However, ketene hydrogen exchange still leads to equivalent frameworks and two states, A_1:A_2, give rise to spin statistics of 1:3. Similar reasoning results in the tunneling states and nuclear spin weights listed in Table 10 for cases A and B. The spectral data are consistent only with case C, where intensity measurements of transitions exhibiting no ketene splitting clearly show the 15:21 spin statistics for CH_2CO–*trans*-CHD=CHD and the approximately 1:1 spin weights for CH_2CO–CH_2CD_2. In addition, CH_2CO–*cis*-CHD=CHD transitions are doubled with splittings comparable to the splittings assigned to the ketene motion in CH_2CO–C_2H_4 and CH_2CO–CH_2CD_2.

Further spectral evidence for the ethylene tunneling motion exchanging *trans* hydrogen pairs (case C) comes from expected differences in the deuterium hyperfine splitting of the 1_{11}–0_{00} transitions of CH_2CO–*trans*-CHD=CHD and CH_2CO–

Table 10. Tunneling States and Nuclear Spin Statistics of Ketene–Ethylene Complex

isotopic species	tunneling states: ethylene	tunneling states: overall[b]	nuclear spin statistics: ethylene[a]	nuclear spin statistics: overall[b]
		Case A		
CH_2CO–C_2H_4	A:B	A_1:A_2:B_1:B_2	10:6	5:15:3:9
CH_2CO–CD_2CH_2	A:B	A_1:A_2:B_1:B_2	15:21	5:15:7:21
CH_2CO–*trans*-CHDCHD	A″:A′	A_1″:A_2″:A_1′:A_2′	1:1	1:3:1:3
CH_2CO–*cis*-CHDCHD		A_1:A_2		1:3
		Case B		
CH_2CO–C_2H_4	A:B	A_1:A_2:B_1:B_2	10:6	5:15:3:9
CH_2CO–CD_2CH_2	A″:A′	A_1″:A_2″:A_1′:A_2′	1:1	1:3:1:3
CH_2CO–*trans*-CHDCHD	A″:A′	A_1″:A_2″:A_1′:A_2′	1:1	1:3:1:3
CH_2CO–*cis*-CHDCHD	A:B	A_1:A_2:B_1:B_2	15:21	5:15:7:21
		Case C		
CH_2CO–C_2H_4	A:B	A_1:A_2:B_1:B_2	10:6	5:15:3:9
CH_2CO–CD_2CH_2	A″:A′	A_1″:A_2″:A_1′:A_2′	1:1	1:3:1:3
CH_2CO–*trans*-CHDCHD	A:B	A_1:A_2:B_1:B_2	15:21	5:15:7:21
CH_2CO–*cis*-CHDCHD		A_1:A_2		1:3

[a] The tunneling states and nuclear spin statistics are due to ethylene hydrogen exchange (see Figure 2). [b] Both ethylene and ketene internal motion (see Figure 3) give rise to the overall tunneling states and nuclear spin statistics.

CH_2=CD_2. In CH_2CO–*trans*-CHD=CHD, the I_D = 0, 2 hyperfine components are present in the B state lines, while the I_D = 1 components are found in the A state. All hyperfine components are present in both the A″ and A′ state lines of CH_2CO–CH_2CD_2. Fortunately, none of the isotopic species of ketene–ethylene exhibits ketene tunneling splitting for the 1_{11}–0_{00} transition, so complications from the ketene motion do not affect the hyperfine patterns. The effect is to give identical deuterium hyperfine structure for the A″ and A′ states of CH_2CO–CH_2CD_2 and distinctly different hyperfine structure for the A and B states of CH_2CO–*trans*-CHD=CHD. The observed 1_{11}–0_{00} transition of the two deuterated ethylene isotopic species shows this effect. In fact, the hyperfine patterns are quite similar to the 1_{10}–0_{00} transitions of O_3–CD_2CH_2 and O_3–*trans*-CHD=CHD, where it has been shown that ethylene tunneling splitting also arises from exchange of *trans* hydrogen pairs.[4]

E. Electrostatic Modeling. In order to determine which structural form of the ketene–ethylene complex (structure A or B in Table 9) corresponds to the spectroscopically observed most stable form, distributed multipole analysis (DMA)[24,25] was used to calculate the angular geometry of the complex. Analogous calculations were performed for the ketene–acetylene complex[15] to obtain a simple explanation of the distinctly different structures. The distributed multipole model has proved successful in rationalizing and predicting geometries of hydrogen-bonded and other weak complexes.[35-37] In this model, the angular geometry of a dimer is calculated by minimizing the electrostatic interaction energy of unperturbed monomers subject to hard-sphere repulsive constraints. The charge distributions of the monomers are represented by arrays of point multipoles placed on atoms and π-bond centers with numerical values derived from DMA[38] of an *ab initio* charge density. This multisite representation has important mathematical and physical advantages.[24,38] Truncation of the site multipole expansions at the quadrupole level has been found to be adequate for most purposes, although another approach is to truncate the interaction energy at a given order in R, the monomer separation.[39] The repulsive potential that stops the monomers from collapsing together is crudely parametrized by embedding the sites in hard spheres with Pauling van der Waals radii. Again, this simple approach has been found to work well in many circumstances.[24,25,35-37]

In the present case, DMA parameters are required for three molecules. Those for ethylene and acetylene are available from previous work.[24,25] For ketene, an SCF calculation was carried out using the same Dunning basis and a distributed multipole analysis made using the CADPAC program.[40] Interaction sites were placed on all atoms and on the centers of π bonds; hard-sphere repulsive radii were placed on the atoms (r_c = 1.7 Å, r_o = 1.4 Å, r_H = 1.2 Å) and π-bond "hard cylinders" were constructed from additional spheres placed at every quarter bond length and with radii interpolating those of the end atoms. No attempt was made to optimize any of these parameters. The site multipoles are listed for reference in Table 11. The interaction energy was truncated at order R^{-5}, i.e., retaining all terms with four Cartesian indices (charge, hexadecapole, dipole–octopole, quadrupole–quadrupole) in the expansion.

Using the data in the table and the hard-sphere parameters indicated above, the model was applied to the two complexes. For ketene–ethylene, the most stable structure is predicted to have the two heavy-atom chains perpendicular to each other, corresponding to structure A in Table 9 with an electrostatic energy of $U = -8.98 \times 10^{-21}$ J (-2.06×10^{-3} hartree). A secondary minimum at $U = -7.63 \times 10^{-21}$ J (-1.75×10^{-3} hartree) is found for a parallel arrangement, in which the ethylene hydrogens project out of the plane of the heavy atoms; other structures including structure B in Table 9 were much less stable. Some sensitivity to the level of truncation of the multipole series manifested itself at the global minimum in a switch between the perpendicular structure and a very shallow double-minimum potential defining a coordinate for twisting from the perpendicular. For ketene–acetylene, the most stable structure is predicted to be planar and pseudocyclic [$U = -9.46 \times 10^{-21}$ J (-2.17×10^{-3} hartree)], with secondary minima for planar hydrogen-bonded structures in which HCCH attaches to the "lone pair" site on O in ketene [$U = -8.63 \times 10^{-21}$ J (-1.98×10^{-3} hartree)] and for a perpendicular arrangement of the π chains [$U = -8.46 \times 10^{-21}$ J (-1.94×10^{-3} hartee)].

The favored structures are shown in Table 12, from which it is clear that the electrostatic model is in very satisfactory agreement with experiment. Ketene has a mean polarizability of 3.56×10^{-30} m^3 (24 au) in the present basis, and this suggests that dispersion will make a significant contribution to the total binding energy, though not necessarily to its anisotropy, in both complexes. Estimates using an empirical model formulated for van der Waals complexes[41] suggest that anisotropies in induction and dispersion energies are insufficient to change the qualitative predictions of preferred geometry.

(35) Fowler, P. W.; Tole, P. *J. Mol. Struct.* **1988**, *189*, 121.
(36) Buckingham, A. D.; Fowler, P. W. *J. Mol. Struct.* **1988**, *189*, 203.
(37) Kisiel, Z.; Fowler, P. W.; Legon, A. C. *Chem. Phys. Lett.* **1991**, *176*, 446.
(38) Stone, A. J. *Chem. Phys. Lett.* **1981**, *83*, 233.
(39) Price, S. L.; Stone, A. J. *J. Chem. Phys.* **1987**, *86*, 2859.
(40) Amos, R. D. *CADPAC, The Cambridge Analytic Derivatives Package*; SERC: Daresbury, U.K., 1984.
(41) Kisiel, Z. *J. Phys. Chem.* **1991**, *95*, 7605.

Table 11. Distributed Multipole Analyses for Ketene, Ethylene, and Acetylene[a]

	ketene						ethylene		acetylene		
property	H1	C1	BC1	C2	BC2	O	H	C	H	C	BC
x	1.775 11	0	0	0	0	0	1.755 42	0	0	0	0
z	−0.972 18	0	1.241 55	2.483 10	3.580 09	4.677 07	2.328 29	1.265 17	3.139 78	1.136 67	0
q_{00}	−0.01722	0.417 62	−1.026 95	1.563 81	−0.916 57	−0.057 49	−0.037 53	0.075 06	−0.095 50	0.809 47	−1.427 94
q_{10}	−0.039 62	0.499 69	−0.087 45	0.403 16	−0.024 55	−0.286 11	0.118 51	0.178 01	0.417 73	−0.165 53	0
q_{11}	0.224 78	0	0	0	0	0	0.214 46	0	0	0	0
q_{20}	0.012 57	0.909 65	0.659 37	−0.050 88	−0.283 30	0.368 42	0.029 54	0.075 35	−0.213 63	0.019 78	1.135 11
q_{21c}	−0.068 92	0	0	0	0	0	−0.077 17	0	0	0	0
q_{22c}	−0.033 15	0.339 30	0.822 98	0.157 61	−0.367 75	0.329 35	−0.024 27	0.137 45	0	0	0
q_{30}	0.015 54	−0.346 35	0.063 51	−0.107 71	0.062 19	−0.108 22	−0.066 93	0.369 81	0.121 39	−0.769 50	0
q_{31c}	0.00723	0	0	0	0	0	0.010 02	0	0	0	0
q_{32c}	−0.006 05	0.863 72	0.063 75	−0.502 59	−0.028 08	0.051 98	0.022 89	−2.477 65	0	0	0
q_{33c}	−0.011 58	0	0	0	0	0	−0.005 29	0	0	0	0
q_{40}	0.003 15	0.257 39	0.493 83	0.079 90	−0.115 70	0.003 62	0.032 56	0.629 12	0.009 32	0.124 46	0.484 99
q_{41c}	0.002 51	0	0	0	0	0	0.027 29	0	0	0	0
q_{42c}	0.004 46	−0.203 42	0.454 54	0.008 10	−0.172 18	−0.032 99	0.061 70	1.516 12	0	0	0
q_{43c}	−0.021 06	0	0	0	0	0	0.032 39	0	0	0	0
q_{44c}	0.020 02	−0.311 81	−0.006 49	0.005 67	0.000 18	−0.000 03	−0.029 24	0.053 51	0	0	0

[a] All molecules lie in the x,z plane with heavy atoms on the z axis. Coordinates are given in bohr radii. Only one of any set of equivalent sites is listed; multipoles on other members of the set are generated by symmetry. Sites BC are at bond midpoints and are used to improve convergence. The quantitites $q_{lm(c)}$ are the spherical harmonic components in real form of the charge ($l = 0$), dipole ($l = 1$), quadrupole ($l = 2$), octopole ($l = 3$), and hexadecapole ($l = 4$) moments, all in atomic units. Conventions and conversions to Cartesian form are as listed in the following reference. Price, S. L.; Stone, A. J.; Alderton, M. *Mol. Phys.* **1984**, *52*, 1007. All components $q_{lm(s)}$ vanish in this axis system.

Table 12. Geometries of Ketene–Ethylene and Ketene–Acetylene from Distributed Multipole Analysis (DMA)

	ketene–ethylene		ketene–acetylene	
	DMA[a]	exptl[b]	DMA[a]	exptl[c]
R (Å)	3.50	3.46	3.78	3.60
θ_1 (deg)	94	88	78	93
θ_2 (deg)	58	49	58	64

[a] The lowest energy form from DMA. [b] Taken from Table 9, structure A, which most closely resembles the lowest energy form from DMA. [c] The preferred structure A taken from ref 15.

Inspection of contributions to the electrostatic energy shows quadrupole–quadrupole interactions to be dominant and suggests a simple rationalization of the switch from parallel to perpendicular orientations for C≡C → C=C. Acetylene is axially symmetric and has a large and positive quadrupole component along C—C (+5.45 ea_0^2 in the present basis at the SCF level of calculation) and hence negative perpendicular components (2.73 ea_0^2). Ethylene, on the other hand, has smaller positive components in the plane (+1.53 ea_0^2 along CC + 1.30 ea_0^2 across CC) and a negative component (−2.83 ea_0^2) out of the plane. Thus, perpendicularly coordinated ethylene and parallel acetylene present the same favorable profile to the charge distribution of ketene (see Figure 4).

To check this idea, a minimization was carried out in which the hydrocarbons were represented by single, central quadrupole moments and the ketene monomer by a central dipole and quadrupole placed on the CH_2 carbon. As expected, this reproduced the favored orientations of the more complete model, confirming our qualitative picture.

Finally, we note that the electrostatic model is expected to give useful predictions for other complexes of ketene. A simple minimization of ketene–HF using published DMA data for HF[24] predicts H-bonding to O with HF lying at a COF angle of 122° and a COH angle of 124° in the plane bisecting the ketene CH_2 group. This is compatible with the known structure of $H_2C{=}O{-}HF$[42] and is easily reconciled with the lone-pair model of hydrogen bonding[43] when it is remembered that the π bonds are in mutually perpendicular planes in this cumulated system.

IV. Discussion

A. Structure and Internal Motion. Ketene–ethylene and ketene–acetylene[15] are the only known ketene-containing van der Waals complexes. As shown in Figure 5, the monomer planes of the ketene–ethylene complex are crossed, while ketene–acetylene is planar. Electrostatic modeling of the geometries finds that the difference arises from the quadrupole moments of ethylene and acetylene (see Figure 4). Since the quadrupole is the leading molecular multipole moment in these centrosymmetric systems, perpendicular binding of ethylene and parallel binding of acetylene to ketene are favored in the equilibrium structures. A larger van der Waals stretching force constant indicates that $CH_2CO{-}C_2H_4$ is more strongly bound than $CH_2CO{-}C_2H_2$.[15] Using the equation derived for nonplanar asymmetric tops by Millen,[43] the pseudodiatomic model gives a force constant of k_s (N/m) = 3.31(1) for $CH_2CO{-}C_2H_2$ compared to 2.36(1) for $CH_2CO{-}C_2H_2$.

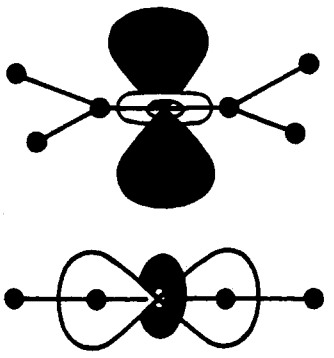

Figure 4. Schematic illustration of the quadrupole moments of acetylene and ethylene. The surfaces are qualitative indications of the electrostatic potential in the region around a point quadrupolar model of each molecule. In acetylene the positive component (unshaded lobes) is along the cc axis; in ethylene it is perpendicular to the molecular plane. Both quadrupoles can be written as combinations of normalized d spherical harmonics. With our wave functions, the acetylene quadrupole is a pure z^2 harmonic with amplitude 5.44 ea_0^2, and the ethylene moment is a mixture of normalized z^2 and $(x^2 - y^2)$ harmonics with amplitudes of 1.53 and 2.39 ea_0^2, respectively.

There are striking similarities in the internal motions of the two ketene complexes. Both $CH_2CO{-}C_2H_4$ and $CH_2CO{-}C_2H_2$ exhibit four tunneling states, and the spectroscopic data provide strong evidence that these states arise from exchange of the ketene and hydrocarbon hydrogens. The spectral data from the deuterated ethylene isotopic species show that *trans* ethylene hydrogen pairs are exchanged by the tunneling motion in the $CH_2CO{-}C_2H_4$ complex. Similar *trans* pairs of ethylene hydrogens

(42) Baiocchi, F. A.; Klemperer, W. *J. Chem. Phys.* **1983**, *78*, 3509.
(43) Legon, A. C.; Millen, D. J. *Chem. Soc. Rev.* **1987**, *16*, 467.

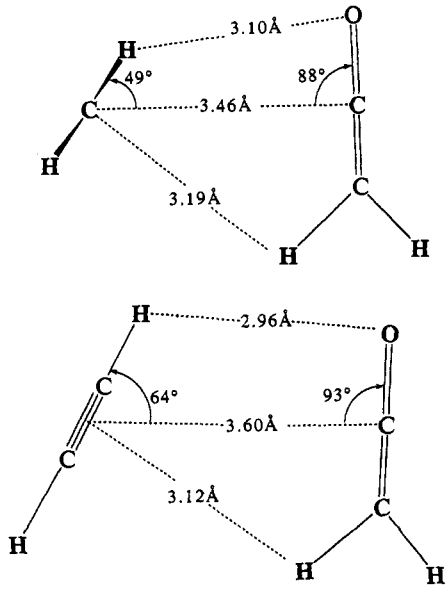

Figure 5. Comparison of the structures of CH_2CO–C_2H_4 and CH_2CO–C_2H_2 complexes determined from microwave data in this work and ref 15, respectively. The dotted lines connecting the monomer subunits identify distances between atoms in the complexes and do not indicate directed interactions.

exchange in O_3–C_2H_4[4] and SO_2–C_2H_4.[33] It is not known whether the internal motions involving ketene and the hydrocarbons are coupled in CH_2CO–C_2H_4 and CH_2CO–C_2H_2. If the tunneling motions are not coupled, then it appears that the barriers to acetylene and ethylene hydrogen exchange are lower than the barriers to ketene hydrogen exchange. A simple C_2 rotation about the molecular axis of ketene (I_a = 1.79 u·Å^2) and the *c* axis of ethylene (I_c = 20.4 u·Å^2) or the *b* axis of acetylene (I_b = 14.3 u·Å^2) gives a much smaller, reduced mass for the ketene motion, which should produce larger spectral splittings in the ketene tunneling states of both complexes. Since the reverse is observed, the ketene barrier to internal rotation is larger than the ethylene and acetylene barriers.

The electrostatic model gives barriers of 471 cm^{-1} for rotation of ethylene about its *a* axis (case A in Figure 2), 113 cm^{-1} for rotation of ethylene about its *c* axis (case C in Figure 2), and 464 cm^{-1} for rotation of ketene about its heavy atom axis (path [1] → [4]). Addition of a model dispersion term does not change these barriers greatly (488, 165, and 586 cm^{-1}) and confirms that the ethylene barrier to rotation about its *c* axis is lowest in energy. Case B in Figure 2 is calculated to become entirely repulsive for rotations of ca. 90°. Therefore, the DMA results are in agreement with the spectroscopic data discussed above. Similar barrier calculations were performed for internal rotation of acetylene and ketene in CH_2CO–C_2H_2 complex. The corresponding barriers for end-over-end rotation of acetylene and rotation about the heavy atom axis of ketene are 241 and 153 cm^{-1}, respectively. Including dispersion in the calculation gives 218 and 159 cm^{-1} for the two barriers.

Though the calculated barrier heights for the two motions in ketene–acetylene complex are similar, the internal rotation of acetylene, which is known to be asociated with a greater splitting, is predicted to have a higher barrier. Interestingly, the model predicts that the rotation of ketene takes place at almost constant intermolecular separation *R*, but the rotation of the acetylene subunit involves changes in *R* of 0.3 Å. This could provide the basis for stronger coupling between the internal rotation of acetylene and overall rotation than expected from barrier heights alone and suggests a rationalization of the two results. This argument does not affect the comparison between experiment and the model for the ketene–ethylene dimer, since the motion C with the lowest barrier is also associated with large calculated changes in *R* (0.27Å).

B. Ketene–Ethylene Complex and (2 + 2) Cycloadditions. The microwave and electrostatic modeling results show that the van der Waals complex of ketene–ethylene has a structure (see Figure 5) which qualitatively resembles the crossed transition state, **I**, proposed by Woodward and Hoffman for a ($2\pi_s$ + $2\pi_a$) cycloaddition.[17] This result is intriguing because it provides another example in cycloaddition chemistry, where the transition-state structure predicted from orbital interactions is similar to the experimental structure of the cycloaddition van der Waals adduct.[4,9,19] Recent high-level computational studies find similar crossed transition states for $CH_2CO + C_2H_4$.[19-22] Although these studies identify different reaction paths, some of which do not involve ($2\pi_s$ + $2\pi_a$) orbital interactions, they all find C–C bond formation more advanced at the carbonyl carbon of ketene than at the methylene carbon in the transition state.[19-23]

If the CH_2CO–C_2H_4 complex is located on a reaction potential surface, it must fall at a large reaction distance, *R* = 3.46 Å, which means that the ketene and ethylene moieties are not close to the transition state on this surface. Yamabe, Minato, and Osamura used frontier molecular orbital interactions with a MP2/6-31G* basis set to investigate both the early stage and transition-state geometries of $CH_2CO + C_2H_4$.[22] The structure calculated for the early stage of the reaction is remarkably similar to the experimental geometry of the complex shown in Figure 5. The molecular planes are crossed with the plane of ethylene tilted toward the oxygen of ketene in both the early stage and transition state structures.[22] This configuration locates the C=C bond of ethylene closer to the carbonyl carbon than to the methylene carbon of ketene. It is important to note that the actual separation of ketene and ethylene is considerably greater in the van der Waals complex than for the theoretical calculation of the structure of the early stage of the reaction. It is likely that a larger basis set is required to describe the binding of ketene to ethylene at van der Waals separations. The structure of ketene–ethylene obtained from the electrostatic model (DMA) agrees with the experimental geometry. Hence, it appears that the DMA model provides a good description of the long-range electrostatic forces that bind ketene to ethylene at large separations.